Nonreciprocal cavities and the time-bandwidth limit: supplementary material

SANDER A. MANN[1,2], **DIMITRIOS L. SOUNAS**[2,3], **AND ANDREA ALÙ**[1,2,4,5,*]

[1]*Photonics Initiative, Advanced Science Research Center, City University of New York, New York 10031, USA*
[2]*Department of Electrical and Computer Engineering, The University of Texas at Austin, Austin, Texas 78705, USA*
[3]*Present address: Department of Electrical and Computer Engineering, Wayne State University, Detroit, Michigan 48202, USA*
[4]*Physics Program, Graduate Center, City University of New York, New York 10016, USA*
[5]*Department of Electrical Engineering, City College of The City University of New York, New York 10031, USA*
Corresponding author: aalu@gc.cuny.edu

This document provides supplementary materials to the Research Article "Nonreciprocal Cavities and the Time-Bandwidth Limit," https://doi.org/10.1364/OPTICA.6.000104. We present additional derivations for the identities given in the main text, details on the nonreciprocal waveguide and cavity geometries, and more information on the simulation methods we have used to obtain our results.

1. The time-bandwidth product

Starting from Eq. 4 in the main text, the stored energy of the resonance is given by:

$$|a(\omega)|^2 = \frac{\left|\mathbf{k}^{\mathrm{T}}\mathbf{s}_+\right|^2}{(\omega-\omega_0)^2+\gamma^2}. \qquad \textbf{(S1)}$$

The full-width, half-maximum of this Lorentzian curve is given by 2γ. Similarly, from Eq. 1 in the main text, it follows that if the cavity has a nonzero amplitude a_0 at $t = 0$ without the presence of an incoming wave, it evolves in time as

$$a(t) = a_0 \exp(i\omega_0 t) \exp(-\gamma t). \qquad \textbf{(S2)}$$

Here, the lifetime of the resonance Δt is given by the time it takes the resonance amplitude to reach $|a_0|e^{-1}$: $\Delta t = 1/\gamma$. Taking the product of the lifetime and bandwidth, we thus find $\Delta t \Delta \omega = 2$.

2. Proofs for nonreciprocal CMT identities

Here we provide proofs for the identities shown in the main text, which we repeat here for clarity

$$\tilde{\mathbf{C}} = \mathbf{C}^{\mathrm{T}} \qquad \textbf{(5a)}$$

$$\tilde{\mathbf{d}} = \mathbf{k} \qquad \textbf{(5b)}$$

$$\tilde{\mathbf{k}} = \mathbf{d} \qquad \textbf{(5c)}$$

$$\tilde{\gamma}_r = \gamma_r \qquad \textbf{(5d)}$$

$$\mathbf{C}^{\mathrm{T}}\mathbf{d}^* = -\mathbf{k} \qquad \textbf{(5e)}$$

$$\mathbf{d}^{\dagger}\mathbf{d} = \mathbf{k}^{\dagger}\mathbf{k}. \qquad \textbf{(5f)}$$

Before proving these relationships, it is important to point out the consequence of a time-reversal operation on general amplitudes of the mode and cavity amplitudes: performing a time-reversal operation leads to $T: \mathbf{s}_+ \to \mathbf{s}_-^*$, $T: \mathbf{s}_- \to \mathbf{s}_+^*$, and $T: a \to a^*$, since it effectively conjugates the temporal exponent in each amplitude and reverses the direction of any vector (such as the propagation vector). In the following we provide the proofs not in order of Eqs. 5, but in an order that makes more sense with respect to interdependencies. These proofs are based on the assumption that the mode profile and frequency are not affected by the time-reversal operation, and for Eqs. 4b,c,e closely follow the proofs for the reciprocal system [1].

Eq. 5a: $\tilde{\mathbf{C}} = \mathbf{C}^{\mathrm{T}}$

The first relationship can be proven simply by considering reflection strongly detuned from resonance, so that $\mathbf{s}_- = \mathbf{C}\mathbf{s}_+$. Under a time-reversal operation, we then find $\mathbf{s}_+^* = \tilde{\mathbf{C}}\mathbf{s}_-^*$. Taking the conjugate, left-multiplying by $\left(\tilde{\mathbf{C}}^*\right)^{-1}$, and using that $\mathbf{C}$ is unitary if the direct pathway is lossless, we find $\tilde{\mathbf{C}} = \mathbf{C}^{\mathrm{T}}$.

Eq. 5d: $\tilde{\gamma}_r = \gamma_r$

To prove Eq. 5d, we again invoke the time-reversed scenario of a decaying cavity. Without input, $\mathbf{s}_+ = 0$, there are no reflections in the time-reversed case: $\tilde{\mathbf{s}}_- = \mathbf{s}_+^* = 0$. Also, as mentioned earlier, the incident signal in the time-reversed case is $\tilde{\mathbf{s}}_+ = \mathbf{s}_-^*$. Hence, we can write for Eq. 2: $\tilde{\mathbf{C}}\mathbf{s}_-^* + \tilde{\mathbf{d}}a^* = 0$. Given that $\mathbf{s}_-^* = \mathbf{d}^*a^*$, we find $\tilde{\mathbf{C}}\mathbf{d}^* = -\tilde{\mathbf{d}}$, which, when invoking unitarity of $\mathbf{C}$, yields $\tilde{\mathbf{d}}^{\dagger}\tilde{\mathbf{d}} = \mathbf{d}^{\dagger}\mathbf{d}$, and thus Eq. 5d.

Eqs. 5b,c: $\tilde{\mathbf{d}} = \mathbf{k}$ and $\tilde{\mathbf{k}} = \mathbf{d}$

To prove Eqs. 4b,c, consider a lossless cavity with an initial amplitude decaying into the ports, while $\mathbf{s}_+ = 0$. In this scenario, both a and $\mathbf{s}_-$ decay exponentially with complex frequency $\omega_0 - i\gamma$. If we then reverse time, we excite the cavity with an exponentially growing wave with amplitude $\tilde{\mathbf{s}}_+ = \mathbf{s}_-^*$ and frequency $\omega_0 + i\gamma$. Now, starting from the equation of motion $(i\omega - i\omega_0 + \gamma)a = \mathbf{k}^T\mathbf{s}_+$, we find for the time-reversed scenario at frequency $\omega = \omega_0 + i\tilde{\gamma}$

$$(-i(\omega_0 + i\tilde{\gamma}) + i\omega_0 + \gamma)a^* = \tilde{\mathbf{k}}^T\mathbf{s}_-^*. \quad \textbf{(S3)}$$

Using $\gamma = \gamma_r$ and $\tilde{\gamma}_r = \gamma_r$ (which we have just shown), yields $2\gamma_r = \tilde{\mathbf{k}}^T\mathbf{d}^*$. Taking the complex conjugate of $2\gamma_r = \tilde{\mathbf{k}}^T\mathbf{d}^*$ and combining it with $2\gamma_r = \mathbf{d}^\dagger\mathbf{d}$, we find

$$(\tilde{\mathbf{k}}^\dagger - \tilde{\mathbf{d}}^\dagger)\mathbf{d} = 0. \quad \textbf{(S4)}$$

As long as $\mathbf{d}$ is a non-zero vector, this implies $\tilde{\mathbf{k}} = \mathbf{d}$. Starting from the time-reversed scenario and following the same analysis, we can also confirm that $\tilde{\mathbf{d}} = \mathbf{k}$.

Eq. 5e: $\mathbf{C}^T\mathbf{d}^* = -\mathbf{k}$

In the derivation for Eq. 5d we showed that $\tilde{\mathbf{C}}\mathbf{d}^* = -\tilde{\mathbf{d}}$. Combining this result with Eq. 5b, $\tilde{\mathbf{d}} = \mathbf{k}$, we immediately find Eq. 5e.

Eq. 5f: $\mathbf{d}^\dagger\mathbf{d} = \mathbf{k}^\dagger\mathbf{k}$

Finally, by using the fact that $\mathbf{C}$ is unitary, we obtain Eq. 5f from Eq. 5e: $\mathbf{d}^\dagger\mathbf{d} = \mathbf{k}^\dagger\mathbf{k}$. It is interesting to point out that there are various ways to derive this fluctuation-dissipation relation: one may also prove it using balance of power, or more rigorously, using stochastic methods [2]. Furthermore, it is important to point out that in the case of internal absorption, $\gamma_i > 0$, the full fluctuation-dissipation relation needs to be amended to include absorptive dissipation as well.

In this context, we should stress that while these proofs rely on the unitarity of $\mathbf{C}$, the relations in Eq. 5 can also be more generally applied to lossy systems by considering loss as (an) additional port(s). This is specifically demonstrated by a heuristic derivation of Eq. 5e for the system with a dissipative wedge mode in Section 5 of the Supplementary Information.

3. Details of cavity geometries and materials

The unidirectional waveguides we use to study non-reciprocal cavities are based on the work by Shen et al. [3,4]. The materials used in all of our simulations are the same: silicon (Si) and indium-antimonide (InSb). We use a constant permittivity for Si: $\varepsilon_{Si} = 11.68\,\varepsilon_0$, and for InSb we use the transversely ($\hat{z}$) magnetized permittivity tensor [3]:

$$\boldsymbol{\varepsilon}_{InSb} = \varepsilon_0\varepsilon_\infty \begin{pmatrix} \varepsilon_1 & i\,\varepsilon_2 & 0 \\ -i\,\varepsilon_2 & \varepsilon_1 & 0 \\ 0 & 0 & \varepsilon_3 \end{pmatrix} \quad \textbf{(S5)}$$

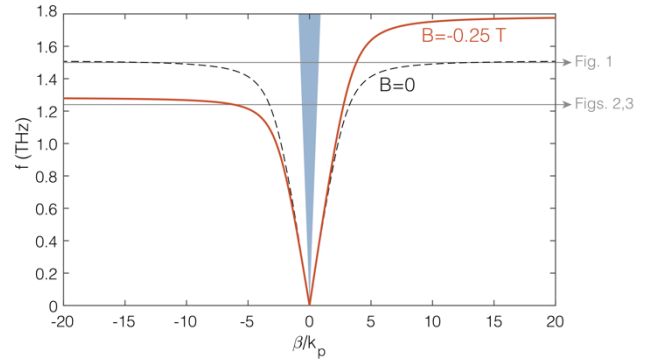where $\varepsilon_\infty = 15.6\,\varepsilon_0$ and

Fig. S1: Dispersion of the surface plasmon. Without magnetic bias the dispersion is shown by the dashed black curve, and is symmetric about *k=0*. By biasing the sample with a magnetic field, propagation forward and backward obtain different dispersion curves. Over a large range of frequencies (almost 0.5 THz) there is a unidirectional gap. The operating frequencies for Fig. 2 and Figs. 3,4 are shown with the gray curves, and the light cone is shown in blue. The propagation vector is normalized to the wavenumber at the plasma frequency $\omega_p = 4\pi\ 10^{12}$ rad/s.

$$\varepsilon_1 = 1 - \frac{(\omega+i\nu)\omega_p^2}{\omega((\omega+i\nu)^2 - \omega_c^2)} \quad \textbf{(S6a)}$$

$$\varepsilon_2 = \frac{\omega_c\omega_p^2}{\omega((\omega+i\nu)^2 - \omega_c^2)} \quad \textbf{(S6b)}$$

$$\varepsilon_3 = 1 - \frac{\omega_p^2}{\omega((\omega+i\nu)^2 + i\nu)} \quad \textbf{(S6c)}$$

Here $\omega_p = 4\,\pi \times 10^{12}$ rad/s is the plasma frequency, $\nu = 5 \times 10^{-3}\omega_p$ rad/s is the collision frequency, and $\omega_c = eB/m = 0.25\omega_p$ is the cyclotron frequency (corresponding to a static magnetic field bias of 0.25 T in the $-\hat{z}$ direction).

In all simulations the waveguide has the same dimensions: the total height of the waveguide is 30 μm, filled with 18 μm of InSb at the bottom and 12 μm of Si at the top. The bottom and top walls of the waveguide are perfect electric conductors (see the next section). The dispersion of this single-mode waveguide is shown in Fig. S1, both without magnetic bias (black dashed lines) and with magnetic bias (orange solid lines). The unidirectional regime, where there is only propagation in the positive direction, is clearly visible.

For Fig. 2 in the main text we place a cavity behind the termination of the waveguide, which is 20×30 μm and resonant at 1.52 THz. The cavity is connected to the waveguide through a small opening with height of 0.5 μm and a width of 0.1 μm. See Fig. S2a for a schematic drawing of this geometry. We operate the waveguide in the unidirectional regime, with a pulse centered at 1.5 THz and a bandwidth of 0.16 THz (see next section).

For Fig. 3 in the main text, we operate the waveguide in the bidirectional regime, below ~1.25 THz [4]. We increase the cavity size to 20×35.4 μm so that it is resonant at 1.24 THz, and while we maintain the opening at the same position in the waveguide (3 μm) from the top wall, we shift the cavity upwards so that the opening is closer to the middle of the cavity (which increases the cavity Q-factor). The displacement between the middle plane of the cavity
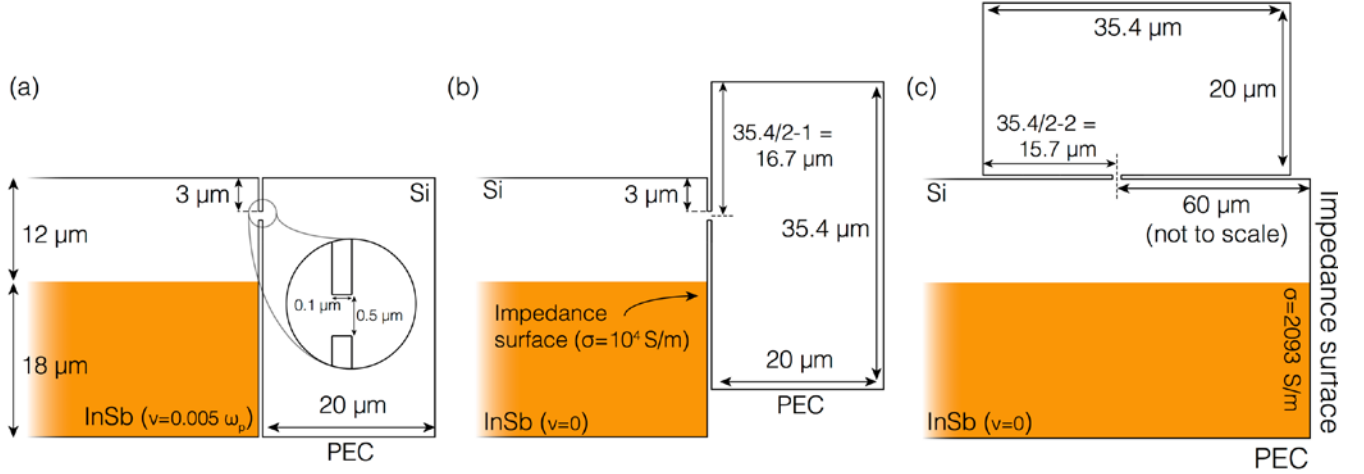
Figure S2: (a) Schematic for the first cavity discussed in the main text (and in Fig. 1), where the inset shows the geometry of the cavity opening. (b) Schematic for the second system discussed in the main text (and in Fig. 2), where almost everything is identical as in the previous cavity except for a displacement of the cavity and a larger size. (c) The cavity is the same as in (b), except that now the cavity is on top and slightly displaced from the opening. In the waveguide, the opening is placed at a position where the forward and backward fields cancel out.

and the middle of the opening is 2 μm. For simplicity of analysis (see Section 4) we set the collision frequency to 0 but have changed the PEC termination to a lossy impedance boundary condition with a conductivity of 10^4 S/m and $\varepsilon = \varepsilon_0$. See Fig. S2b for schematic details on this geometry.

The final geometry we have studied, discussed in Fig. 4 in the main text, has identical features to the previous cavity, except that the cavity is now positioned on top of the waveguide and that the conductivity of the termination has been reduced to 2093 S/m. The cavity opening is centered 60 µm away from the termination, where there is a zero in the magnetic field (see Fig. S2c).

4. Anisotropic FDTD algorithm

To perform full-wave simulations of the cavity in the time-domain we employ a home-built FDTD algorithm. For the geometries of interest, it is important for the algorithm to support i) Drude-model dispersion, and ii) anisotropic materials. To incorporate anisotropic Drude dispersion, we employ the auxiliary differential equation (ADE) method, which captures the dispersion in an additional equation for the current density [5] but implemented so that it supports anisotropic materials. Starting from Ampere's law in differential form:

$$\nabla \times \mathbf{H} = \varepsilon_0 \frac{\partial}{\partial t}\mathbf{E} + \mathbf{J}, \qquad \text{(S7)}$$

where

$$\mathbf{J} = i\omega\mathbf{P} = i\omega\varepsilon_0\boldsymbol{\chi_e}\mathbf{E}. \qquad \text{(S8)}$$

From the permittivity of InSb in Supplementary Section 3, we can write for the susceptibility:

$$\boldsymbol{\chi_e} = \frac{\varepsilon_\infty\omega_p^2}{\omega((\omega+i\nu)^2-\omega_c^2)}\begin{pmatrix} -(\omega+i\nu) & i\omega_c \\ -i\omega_c & -(\omega+i\nu) \end{pmatrix}, \qquad \text{(S9)}$$

so we find for the current density:

$$\mathbf{J} = \frac{\varepsilon_0\varepsilon_\infty\omega_p^2}{((\omega+i\nu)^2-\omega_c^2)}\begin{pmatrix} -i(\omega+i\nu) & -\omega_c \\ \omega_c & -i(\omega+i\nu) \end{pmatrix}\mathbf{E} \qquad \text{(S10)}$$

Inverting the matrix in this equation to bring it to the other side:

$$\frac{-1}{(\omega+i\nu)^2-\omega_c^2}\begin{pmatrix} -i(\omega+i\nu) & -\omega_c \\ \omega_c & -i(\omega+i\nu) \end{pmatrix}\mathbf{J} =$$
$$\frac{\varepsilon_0\varepsilon_\infty\omega_p^2}{(\omega+i\nu)^2-\omega_c^2}\mathbf{E} \qquad \text{(S11)}$$

Cancelling out the denominator, and using $i\omega\mathbf{J} \to \frac{\partial\mathbf{J}}{\partial t}$, we finally find:

$$\frac{\partial}{\partial t}\mathbf{J} + \begin{pmatrix} -\nu & -\omega_c \\ \omega_c & -\nu \end{pmatrix}\mathbf{J} = \varepsilon_0\varepsilon_\infty\omega_p^2\mathbf{E}. \qquad \text{(S12)}$$

This auxiliary differential equation incorporates the dispersion, and when converted into an update equation it can be added to a regular FDTD algorithm. We use the material parameters as presented in the previous section, and a mesh of 10 by 10 nm.

5. Heuristic derivation of CMT for cavity and nonreciprocal waveguide

In the unidirectional waveguide discussed in Fig. 2 in the main text there is no reflected power over the whole frequency range of interest, and the direct reflection coefficient C is therefore 0. We thus obtain an additional coefficient for the direct excitation of the wedge mode (which is responsible for absorbing the incident power), $|C_w|^2 = 1 - |C|^2$, so that without the cavity the power absorbed by the wedge mode is $P_w = |C_w s_+|^2$. While there is no backwards mode, even in the case of a lossless cavity as in Fig. 2 in the main text, the resonance can (and must be able to) dissipate power by exciting the wedge mode, which for the cavity results in an additional loss rate γ_w:

$$\frac{d}{dt}a = (i\omega_0 - \gamma_r - \gamma_i - \gamma_w)a + k_r s_+. \qquad \textbf{(S13)}$$

It turns out that it is crucial to consider that both the incident wave and the resonance can excite the wedge mode, and that in due process they can thus interfere. The total power absorbed by the wedge mode in general is therefore given by

$$P_w = |C_w s_+ + d_w a|^2 \qquad \textbf{(S14)}$$

where d_w relates the excitation of the wedge mode to the cavity amplitude, with $|d_w|^2 = 2\gamma_w$ (which can be shown from balance of power in the case that $\gamma_r = \gamma_i = 0$). If we then reconsider balance of power

$$|s_+|^2 = |s_-|^2 + 2\gamma_i|a|^2 + P_w, \qquad \textbf{(S15)}$$

and substitute s_- and $\boldsymbol{P_w}$:

$$|s_+|^2 = |Cs_+ + d_r a|^2 + 2\gamma_i|a|^2 + |C_w s_+ + d_w a|^2, \qquad \textbf{(S16)}$$

which becomes

$$|s_+|^2 = (|C|^2 + |C_w|^2)|s_+|^2 + 2(\gamma_i + \gamma_r + \gamma_w)|a|^2$$
$$+2\mathrm{Re}(C^* s_+^* d_r a) + 2\mathrm{Re}(C_w^* s_+^* d_w a). \qquad \textbf{(S17)}$$

Grouping together and dividing out the input wave leads to

$$(\gamma_i + \gamma_r + \gamma_w)|a|^2 + \mathrm{Re}(C^* s_+^* d_r a)$$
$$+\mathrm{Re}(C_w^* s_+^* d_w a) = 0. \qquad \textbf{(S18)}$$

Inserting the equation for the cavity amplitude and setting $\omega = \omega_0$, we find:

$$\frac{(\gamma_i + \gamma_r + \gamma_w)|k_r s_+|^2}{(\gamma_i + \gamma_r + \gamma_w)^2} + \mathrm{Re}\left(\frac{C^* s_+^* d k_r s_+}{(\gamma_i + \gamma_r + \gamma_w)}\right)$$
$$+\mathrm{Re}\left(\frac{C_w^* s_+^* d_w k_r s_+}{(\gamma_i + \gamma_r + \gamma_w)}\right) = 0, \qquad \textbf{(S19)}$$

which becomes

$$k_r^* k_r + \mathrm{Re}(C^* d k_r) + \mathrm{Re}(C_w^* d_w k_r) = 0. \qquad \textbf{(S20)}$$

Considering that $k_r^* k_r$ is real, we can write:

$$-k_r^* = C_w^* d_w + C^* d. \qquad \textbf{(S21)}$$

This equation is equivalent to Eq. 5d in the main text for this two-port system and it demonstrates that k and d can indeed be different, as also observed in the simulation, as long as there is an additional channel. In the case that d=0 (when the waveguide is unidirectional), we again find that $|k_r| = |d_w|$, which means that power can enter the cavity at the same rate that the cavity can dissipate it via the wedge mode.

We stress again that it is crucial for the input and cavity to be able to interfere at the wedge. If this were not the case, and for example the wedge mode would dissipate incoherently as $P_w = |C_w s_+|^2 + |d_w a|^2$, this would result again in the requirement $|d_r| = |k_r|$. In fact, in this scenario it is not necessary to consider the term γ_w separately from γ_i, and a general description can be obtained without explicit consideration of P_w and γ_r. This fact makes the wedge mode alike an additional channel, rather than simply an additional dissipative process.

6. Using COMSOL for nonreciprocal waveguides

For the results in Figs. 3,4 (as well as the intensity plots in Fig. 2) in the main text we use COMSOL rather than our FDTD algorithm, because we are interested in complex amplitudes of the ingoing and outgoing waves with respect to the cavity amplitude. In the following we describe how to use COMSOL for simulations with nonreciprocal media and the fitting procedure to obtain the coefficients discussed in the main text. For reciprocal media it would be most convenient to use COMSOL port boundary condition to launch and accept incoming and outgoing modes and to determine the reflection coefficient from the structure. However, COMSOL's numerical ports do not work with nonreciprocal waveguides, because the incoming and outgoing modes are different. We therefore applied the following procedure to obtain the complex mode and cavity amplitudes, assuming that we are modeling one of the structures in Fig. S2:

1. Create the geometry and add a port on the left end of the waveguide, with "wave excitation" set to "on".
2. To the left of where this port is, add a small second domain that is essentially an extension of the waveguide. Create a second Electromagnetic Waves, Frequency Domain that applies only to this domain and make sure that in the main physics domain this waveguide extension is excluded.
3. In the second physics domain, set this waveguide extension up so that there is a port on the right boundary (overlapping with the port in the main physics domain). All other boundaries can be PEC.
4. Back in the first domain, add a second port on the same boundary, set it to a user defined port and modify the expressions for the electric mode field and propagation constant so that they are obtained from the other physics domain: e.g. "emw2.tEmodex_3", etc. Make sure wave excitation is set to "off" in this port. In this main physics domain there are now separate ports for ingoing and outgoing modes.
5. Although not strictly necessary (and slightly more complicated), it is possible to modify the weak expressions in the launching port so that it does not try to accept the returning mode. It requires adding an additional port for the electric field (following a similar procedure as before, but now in the same physics domain), and then add 0* before all if's in emw.PortConstrx, emw.PortConstry, emw.PortConstrz, emw.PortConstrx_weak, emw.PortConstry_weak, emw.PortConstrz_weak, and the weak expression for the domain computation.
6. Use an overlap integral on the input boundary to determine the input and output phase and amplitudes. Because these modes are nonreciprocal, the overlap integral is different [6]:

$$c_m = \frac{\iint(\mathrm{E_{Tm}} \times \mathrm{H_T} + \mathrm{E_T} \times \mathrm{H_{Tm}}) \cdot \hat{z}dA}{2\iint(\mathrm{E_{Tm}} \times \mathrm{H_{Tm}}) \cdot \hat{z}dA} \qquad \textbf{(S22)}$$
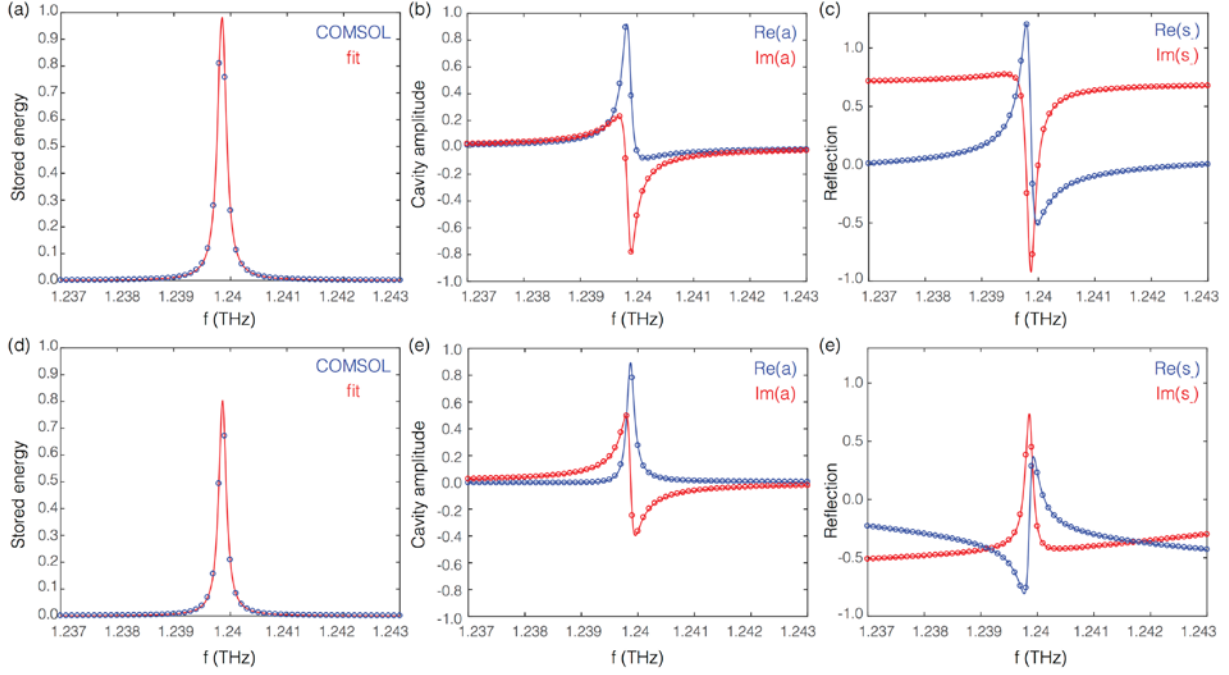
Figure S3: Fits of the stored energy (a), complex mode amplitude (b), and reflected amplitude (c) of a reciprocal cavity (without a magnetic bias). The bottom row of plots (d-e) shows the same, except for a nonreciprocal cavity (magnetic bias turned on). In all cases the fit is excellent, while fitting only one parameter (b,c,e,f). In (a,d) we fit three parameters: the loss rate, center frequency, and maximum stored energy (which we don't use in our analysis).

Here, $\mathbf{E}_{Tm}$ and $\mathbf{H}_{Tm}$ are the transverse mode profiles, while $\mathbf{E}_T$ and $\mathbf{H}_T$ are the transverse field profiles of the full solution.

7. Having obtained the input and output complex amplitudes, we can obtain the complex cavity amplitude from an integral over the stored electromagnetic energy in the cavity (due to the small opening and PEC walls virtually no energy is stored outside of the cavity) for the amplitude, and a field monitor in the center of the cavity for the phase.

7. Fitting simulations with the coupled-mode theory model

We now describe the fitting procedure to obtain the complex coefficients reported in the main text. First, starting with the system shown in Fig. S2b but without a magnetic field bias (so that it is reciprocal), we perform a frequency sweep for three different cavity sizes: one for the resonant cavity size ($20 \times 35.4 \, \mu$m), and for cavity sizes one micron longer and shorter. We use these non-resonant cavities to determine the direct reflection path, by averaging $C = S_-/S_+$ for both simulations. Then, we obtain ω_0 and γ from a lorentzian fit of the stored energy in the cavity, which is shown in Fig. S3a: $\omega_0 = 1.24$ THz and $\gamma = 96.7$ MHz. To obtain k_r we then proceed to the complex cavity amplitude, which we fit using

$$a = \frac{k_r s_+}{i(\omega - \omega_0) + \gamma}. \qquad \textbf{(S23)}$$

We use ω_0 and γ from the previous fit and s_+ is input from COMSOL, and hence only k_r is a fitting parameter (shown in red). The fit of the complex cavity amplitude is shown in Fig. S3b, for $k_r = (2.22 - 1.78) \times 10^4 \sqrt{\text{rad/s}}$.

To obtain d_r we fit the reflected amplitude:

$$s_- = C s_+ + d_r a. \qquad \textbf{(S24)}$$

Here, again, d_r is the only fit parameter (shown in red), and the rest we have obtained directly from COMSOL. Fig. S3c shows the resulting fit, for $d_r = (2.22 - 1.79) \times 10^4 \sqrt{\text{rad/s}}$. As expected, $k_r = d_r$ but for a very small difference (the ratio is $\frac{d_r}{k_r} = 1.0010 - 0.0007i$). The small differences most likely originate from estimating C (by changing the cavity size) and a (by assuming that all of the stored energy is inside the cavity). The fact that we find $k_r = d_r$ in the reciprocal regime thus validates our method. If we now turn the magnetic field bias on again, we find the fits shown in Figs. S3d-e, with $\omega_0 = 1.24$ THz and $\gamma = 81.2$ MHz (indicating that the decay rate has changed, which is to be expected given the change in the waveguide mode field profiles). By fitting the complex cavity and reflection amplitudes we find $k_r = (2.65 + 0.308) \times 10^4 \sqrt{\text{rad/s}}$ and $d_r = (0.667 + 2.14) \times 10^4 \sqrt{\text{rad/s}}$. Now, clearly, the values are different: their ratio is $\frac{d_r}{k_r} = 0.34 + 0.77i$.
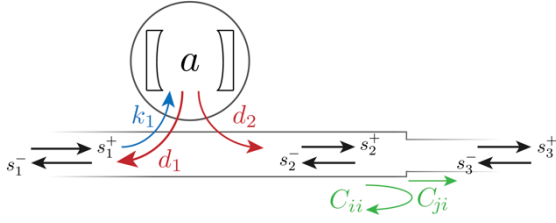
Fig. S4: Schematic illustrating an equivalent system to Fig. 4 in the main text, where we are interested in the effective coupling coefficients between the cavity and ports 1 and 3 which incorporate the effect of the waveguide junction.

8. Effective input and output coefficients

In Fig. 4 in the main text we investigate a cavity coupled to a waveguide with a junction/termination at a different location, and we consider the signal transmitted through the junction (or dissipated in the termination) as a direct output port of the cavity. In reality, the cavity couples to left- and right-propagating waveguide modes, the latter of which undergoes multiple reflections between the termination and the cavity. Here, we will show that one can write effective coupling coefficients that still follow the time-reversal rules in Eqs. 5b,c.

Consistent with the schematic in Fig. S4, we consider a cavity with resonant amplitude a that decays into a waveguide with coefficients d_1 and d_2. We assume that the coupling of the cavity to the waveguide represents a negligible perturbation of the off-resonant excitation, so that the direct scattering matrix is simply the backward identity matrix. We then find for the waveguide section containing the cavity:

$$\begin{pmatrix} s_1^- \\ s_2^+ \end{pmatrix} = \begin{pmatrix} 0 & 1 \\ 1 & 0 \end{pmatrix} \begin{pmatrix} s_1^+ \\ s_2^- \end{pmatrix} + \begin{pmatrix} d_1 \\ d_2 \end{pmatrix} a. \tag{S25}$$

We may express this relation in terms of a scattering matrix $\mathbf{S}$ by inserting Eq. 4 in the main text:

$$\mathbf{S} = \begin{pmatrix} 0 & 1 \\ 1 & 0 \end{pmatrix} + \frac{d\mathbf{k}^\mathrm{T}}{i(\omega_0 - \omega) - \gamma}. \tag{S26}$$

Then, to find the effective output coupling coefficients, we simply solve for the cavity amplitude due to excitation at s_1^+ or s_3^-, considering the full system. Starting with excitation from s_3^-, we find by taking multiple reflections into account:

$$a \propto k_2 s_2^- = k_2(C_{12}e^{ik^- L}s_3^- +$$
$$C_{12}e^{ik^- L}S_{22}e^{-ik^+ L}C_{11}e^{ik^- L}s_3^- + \cdots) \tag{S27}$$

Here we distinguish, due to nonreciprocity between propagation constants in the forward (+) and backward (-)

direction. Writing $k_\Delta = k^+ - k^-$, we can more concisely write for the effective coupling coefficient:

$$k_{3,eff} = \frac{k_2 C_{12} e^{ik^- L}}{1 - S_{22}C_{11}e^{-ik_\Delta L}} \tag{S28}$$

Likewise, following a similar procedure for excitation from port s_1^+, we find:

$$a \propto k_1 s_1^+ + k_2 s_2^- = k_1 s_1^+ + k_2(C_{11}e^{-ik_\Delta L} +$$
$$(C_{11}e^{-ik_\Delta L})^2 S_{22} + (C_{11}e^{-ik_\Delta L})^3 S_{22}^2 + \cdots)S_{21}s_1^+, \tag{S29}$$

which leads to

$$k_{1,eff} = k_1 + \frac{k_2 C_{11} e^{-ik_\Delta L} S_{21}}{1 - S_{22}C_{11}e^{-ik_\Delta L}}. \tag{S30}$$

We now have expressions for the effective incoupling coefficients. To find the effective outcoupling coefficients, we start from a given cavity amplitude and determine the radiated power into each port:

$$s_1^- = d_1 a + S_{12}C_{11}e^{-ik_\Delta L}d_2 a +$$
$$S_{12}S_{22}(C_{11}e^{-ik_\Delta L})^2 d_2 a + \cdots, \tag{S31}$$

which leads to

$$d_{1,eff} = d_1 + \frac{d_2 S_{12}C_{11}e^{-ik_\Delta L}}{1 - S_{22}C_{11}e^{-ik_\Delta L}}. \tag{S32}$$

Finally, we find for the last effective coefficient:

$$s_3^+ = C_{21}e^{-ik^+ L}d_2 a + C_{21}e^{-ik^+ L}(S_{22}C_{11}e^{-ik_\Delta L})d_2 a +$$
$$C_{21}e^{-ik^+ L}(S_{22}C_{11}e^{-ik_\Delta L})^2 d_2 a + \cdots, \tag{S33}$$

which results in:

$$d_{3,eff} = \frac{d_2 C_{21} e^{-ik^+ L}}{1 - S_{22}C_{11}e^{-ik_\Delta L}}. \tag{S34}$$

We have now found all effective coupling coefficients, and can verify that the same time-reversal rules derived for the regular coupling coefficients still apply. Starting with the time-reversal equivalence between $\mathbf{k}$ and $\tilde{\mathbf{d}}$, we reverse $\mathbf{k}_{\mathbf{eff}}$ in time. This yields:

$$\tilde{k}_{1,eff} = d_1 + \frac{d_2 C_{11} e^{-ik_\Delta L} S_{12}}{1 - S_{22}C_{11}e^{-ik_\Delta L}} \tag{S35}$$

$$\tilde{k}_{3,eff} = \frac{d_2 C_{21} e^{-ik^+ L}}{1 - S_{22}C_{11}e^{-ik_\Delta L}} \tag{S36}$$

Here we have used Eqs. 5 in the main text (including that $\tilde{\mathbf{S}} = \mathbf{S}^{\mathrm{T}}$, which holds for any scattering matrix – not only $\mathbf{C}$). We see that $\tilde{\mathbf{k}}_{eff} = \mathbf{d}_{eff}$. Likewise, reversing $\mathbf{d}_{eff}$ instead yields the analogous Eq. 5b. Similarly, $2\gamma_{\mathrm{r}} = \mathbf{d}_{eff}^{\dagger}\mathbf{d}_{eff}$ and $\mathbf{d}_{eff}^{\dagger}\mathbf{d}_{eff} = \mathbf{k}_{eff}^{\dagger}\mathbf{k}_{eff}$, *i.e.*, treating this system comprising a cavity and a waveguide junction as a simple cavity with two ports is valid. It is, however, interesting to point out one significant difference: in contrast to the real coupling coefficients, the effective coupling coefficients are frequency dependent due to the finite path length between the cavity opening and the waveguide junction. In our simulations, the cavity bandwidth is narrow enough to be able to neglect the frequency dependence of the effective coupling coefficients.

9. References

1. W. Suh, Z. Wang, and S. Fan, IEEE J. Quantum Electron. **40,** 1511 (2004).
2. N.G. van Kampen, *Stochastic Processes in Physics and Chemistry*. (Elsevier, North-Holland, 1992).
3. L. Shen, Y. You, Z. Wang, and X. Deng, Opt. Express **23**, 950 (2015).
4. L. Shen, X. Zheng, and X. Deng, Opt. Express **23**, 11790 (2015).
5. A. Taflove and S. Hagness, *Computational electrodynamics: the finite-difference time-domain method (2nd edition)*. Ch. 9. (Artech House, 2000).
6. P. R. McIsaac, IEEE Trans. Microw. Theory Tech. **39**, 1808 (1991).